Revista Mexicana de Astronomía y Astrofísica, **37**, 213–220 (2001)

WIND POWER SPECTRUM MEASURED AT THE SAN PEDRO MÁRTIR SIERRA

D. Hiriart, J. L. Ochoa, and B. García

Instituto de Astronomía
Universidad Nacional Autónoma de México

Received 2001 February 22; accepted 2001 August 15

RESUMEN

El propósito de este estudio es desarrollar un modelo del espectro de potencias del viento en el sitio elegido para construir el Telescopio Óptico-Infrarrojo Mexicano de nueva tecnología (TIM). El modelo obtenido será de utilidad en el estudio y el diseño de la estructura del telescopio, así como del edificio que lo contendrá. Este artículo presenta los resultados de los primeros análisis de un grupo selecto de datos de viento obtenidos en el sitio a una frecuencia de muestreo de 40 Hz. De cada conjunto de datos seleccionado se determinó su espectro de potencias y se ajustó una relación del tipo $\propto f^{-\gamma}$ para la región de altas frecuencias. En dicha región el índice espectral γ se encuentra en el intervalo de 0.625 a 0.969 y muestra una dependencia con la dirección del viento. El máximo de los espectros obtenidos se encuentra en el intervalo de frecuencias de 0.008 a 0.017 Hz. Nuevos estudios serán necesarios cuando el edificio sea instalado en el lugar debido a los cambios introducidos en la orografía local.

ABSTRACT

The purpose of this study is to develop a wind spectrum model for the site of the new Mexican Optical-Infrared Telescope (TIM) to be installed at the Sierra of San Pedro Mártir. This model will be useful in the study and design of the structure and building that will contain the telescope. This paper summarizes the results of our initial analysis of selected wind data obtained at the site with a sampling frequency of 40 Hz. For each data set we calculated the power spectral density. A power law $\propto f^{-\gamma}$ for the high frequency part of the spectrum was fitted and the spectral index γ was found to be in the range of 0.625 to 0.969, and to depend on the wind direction. The frequency for the maximum of the spectrum lies in the range of 0.008 to 0.017 Hz. These studies should be repeated once the building is installed at the site due to changes in the site topography.

Key Words: **ATMOSPHERIC EFFECTS — SITE TESTING — WIND SPECTRUM**

1. INTRODUCTION

Large aperture telescopes increase the sensitivity and angular resolution of astronomical observations made from the surface of the Earth. However, these instruments are very prone to be disturbed by changes in the local environment, such as temperature, humidity and wind, that might degrade their performance. Among these perturbations, the vibrations induced by the wind are one of the most disturbing factors. These vibrations should be accounted for in the study of the dynamic interactions between the wind and the structure of the telescope, as well as between the wind and the telescope building, in order to minimize them.

Large aperture antennas in the open air, such as those found in large single-dish radio telescopes and arrays, have low natural frequencies that make them susceptible to respond to the spectral contents of the wind and introduce errors in the beam pointing (Smith et al. 2000).

The Institute of Astronomy of the National Autonomous University of Mexico is planning to build a new telescope for the National Observatory. The Observatory is located at the Sierra San Pedro Mártir in

Baja California (México) at a longitude of 115° W, latitude of +31° N, and at an altitude of 2800 m above the sea level. The Mexican Optical-Infrared Telescope (TIM) will have a segmented primary mirror of 6.5 m diameter, and will be optimized to operate at visible and infrared wavelengths. To optimize the design of the structure and building of the telescope it is useful to study the typical spectrum of the wind at this site.

The wind spectrum and, in particular, the amplitude of the fluctuations over different frequency ranges have been measured. That is, for a specific mean wind speed, we have obtained the magnitude of the variations over a specific range of frequencies. One of the objectives of this paper is to find how the wind intensity fluctuations are affected by the local orography of the site.

In this work we repeat the methodology used by Antebi, Zarghamee, & Kan (1997) in order to compare our results to a similar study developed for the mountains of Pico Veleta and Mauna Kea.

This paper is organized in the following way: in § 2 we describe the procedure to obtain the wind velocity data. In § 3 we show the calculated wind power spectrum. In § 4 we present a discussion of the results. In § 5 we summarize the main conclusions of this work.

2. MEASUREMENTS

Figures 1 and 2 show the contour levels and a three dimensional view, respectively, of the site where the anemometer was placed. The site is located at the top of a small hill where some pine trees and small bushes are present. The anemometer was mounted in a metallic mast at 6.8 meters above the ground level.

The wind velocity data were recorded from April 12 to April 27, 2000. The data were taken with a sonic anemometer model USA-1 from the Metek company. At this height, this anemometer can measure a maximum wind speed of 30 m s^{-1}. It was necessary to lower the value of the acceptable signal-to-noise ratio of the measurements from the default value established at the factory.

At every hour a series of 4150 velocity measurements were taken at a sampling rate of 40 Hz. We measured the intensity and the direction of the horizontal component of the wind, the vertical wind intensity, and the sonic temperature. The resolution of the wind intensity was ± 0.01 m s^{-1}, and the resolution for the wind direction, $\pm 0.4°$. The sonic temperature is similar to the absolute temperature; differences are due to water vapor fluctuations in the atmosphere. The resolution of the sonic temperature

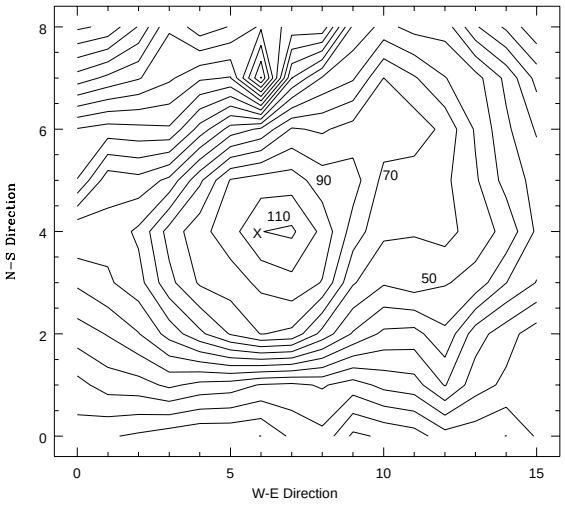

Fig. 1. Contour levels around the site expressed in meters. The anemometer location is marked by a cross.

is ± 0.01 K.

We selected six cases from data sampled at a rate of 40 Hz. Each set has a duration of 102.4 seconds

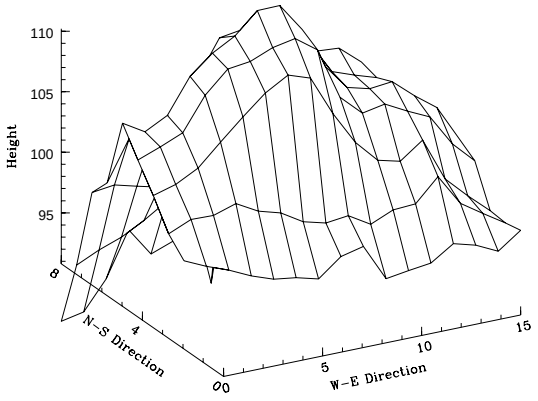

Fig. 2. Three dimensional view of the area around the site. Axes are in meters. The vertical axis is relative to the top which is marked with a height of 110 m.

TABLE 1

DATA OF MEASURED WIND AT SAN PEDRO MÁRTIR SIERRA

	Date	Time	$< V_H >$ (m s^{-1})	σ_H (m s^{-1})	$< \theta >$ (°)	σ_θ (°)	$< V_V >$ (m s^{-1})	σ_V (m s^{-1})
CASE 1	Apr. 12	22:00	2.842	1.08	63.5	11.2	0.21	0.40
CASE 2	Apr. 13	4:00	4.092	0.54	185.6	4.2	0.73	0.25
CASE 3	Apr. 14	0:00	11.13	1.86	205.9	9.9	1.25	1.22
CASE 4	Apr. 17	0:00	9.177	1.39	170.3	8.9	1.11	0.88
CASE 5	Apr. 19	20:00	1.96	0.84	102.6	32.4	0.59	0.364

and contains 4096 data points. The selected cases are shown in Table 1. This table shows for each group: the date and time of the selected sample; the mean wind horizontal speed $< V_H >$, and its dispersion, σ_H; the mean wind direction $< \theta >$, and its dispersion, σ_θ; the mean vertical component of the wind $< V_V >$, and its dispersion, σ_V.

The criterion used to select these cases was that the wind remain fairly constant in direction, so the dependence of the wind spectrum upon the features of the terrain can be determined. It was noticed that, once a wind direction is established, it lasts for several days; thus, only a few data in each direction were obtained.

Figures 3 to 7 show the horizontal and vertical wind intensities and direction versus time for each case shown in Table 1. To simplify these graphs only the data at each second are presented.

3. RESULTS

3.1. *Wind Power Spectrum for San Pedro Mártir*

For each case we calculated a Fast Fourier Transformation (FFT) and obtained the square of the amplitude ($A^2(n)$) as a function of the frequency n. The power spectral density (PSD) of the wind velocity fluctuations is computed as $S(n) = A^2(n)/\Delta n$, where Δn is the sampling frequency f_s multiplied by the number of data points N used in the FFT.

The normalized power spectral density of wind velocity fluctuations $nS(n)/u_f^2$ and the normalized frequency $nz/U(z)$ were computed. The notation used in the calculations is as follows: n is the frequency (Hz), $S(n)$ the power spectral density of the wind velocity fluctuations (m^2 s^{-2} Hz^{-1}), u_f friction velocity (m s^{-1}), z height above the ground (m), $U(z)$ mean wind speed (m s^{-1}) measured at height z.

In the computation, we have used a roughness length $z_0 = 0.025$ m and have also assumed that the wind speeds were measured at $z = 10$ m. The friction velocity is computed using the following equation (Eq. 2.2.18 of Simiu & Scanlan 1966)

$$u_f = \frac{k\,U(z)}{\ln(z/z_0)}\,, \qquad (1)$$

where k is the von Karman's constant ($k = 0.4$). For $k = 0.4$, $z_0 = 0.025$ m and z= 10 m, the friction velocity u_f is 0.0668 U(10m).

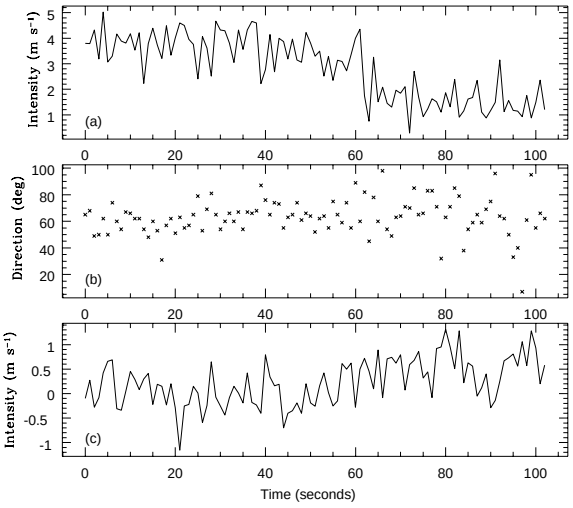

Fig. 3. Wind data for **CASE 1**:(a) horizontal wind intensity; (b)wind direction; (b) vertical wind intensity.

3.2. *Wind Power Spectrum Models*

The power spectrum density (PSD) obtained from the wind data will be compared to three models for the PSD obtained in different conditions:

Davenport spectrum.- This spectrum is based on the average of measurements obtained at various heights above the ground (Davenport 1961)

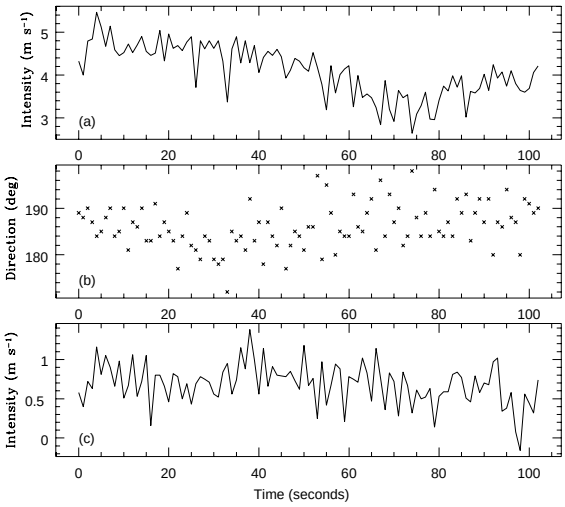

Fig. 4. Same as Figure 3 for **CASE 2**.

$$\frac{n\,S(n)}{u_f^2} \;=\; 4\,\frac{x^2}{(1\,+\,x^2)^{4/3}}\;, \qquad (2)$$

with

$$x = (1200/z)(nz/U(10m)) = (1200/z)f\;, \qquad (3)$$

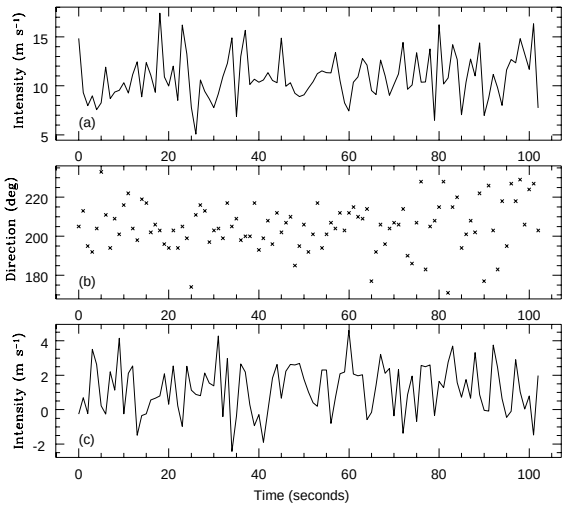

Fig. 5. Same as Figure 3 for **CASE 3**.

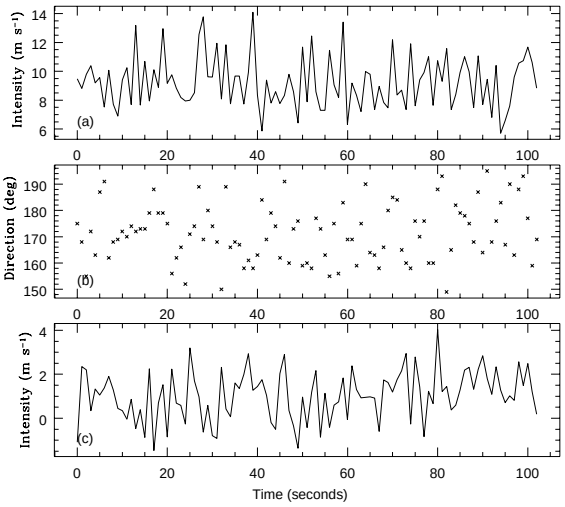

Fig. 6. Same as Figure 3 for **CASE 4**.

where f is the normalized frequency ($nz/U(10m)$).

Spectrum 1. This is a modified Kaimal spectrum (Kaimal et al. 1972) that simulates wind without significant turbulence from local features, such as the effect of a cliff. The selection of this spectrum is discussed in Antebi (1997)

$$\frac{n\,S(n)}{u_f^2} \;=\; \frac{100\,f}{(0.44\,+\,33f)^{5/3}}\;. \qquad (4)$$

Spectrum 2. This spectrum is a best–fitted curve based on the data measured by Antoniou & Asimakopoulos at a height of 30.5 m (Antoniou & Asimakopoulos 1992) and simulates wind with some turbulence from local features such as the effect of a cliff. The selection of this spectrum is discussed in Antebi (1997)

$$\frac{n\,S(n)}{u_f^2} \;=\; \frac{18\,f}{(0.44\,+\,5f)^{5/3}}\;. \qquad (5)$$

Figure 8 shows the normalized power spectral density for these three models. For frequencies larger than $0.1f$ the slope of the three different models is the same ($\propto f^{-\frac{2}{3}}$). In this work we are interested in finding contributions to the wind spectrum at these high frequencies. Figures 9 through 13 show a comparison between the PSD obtained at San Pedro Mártir and the three models for the PSD.

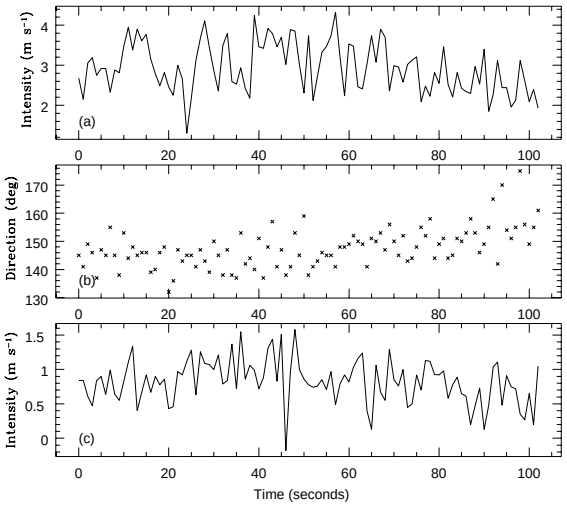

Fig. 7. Same as Figure 3 for **CASE 5**.

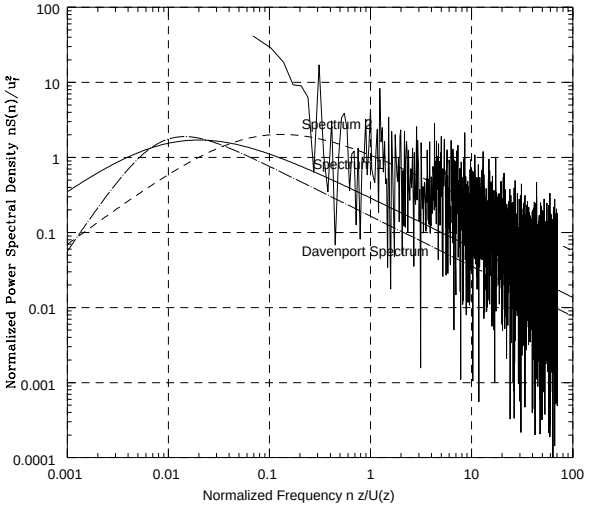

Fig. 9. Power Spectral Density for the wind velocity fluctuations for **CASE 1**.

4. DISCUSSION

From Figs. 9 and 13 it is noticed that, considering the amount of energy, the power spectral density curves for Case 1 and Case 5 follow the general trend of Spectrum 1, while Figs. 10 to 12 follow the general trend of a Davenport's spectrum.

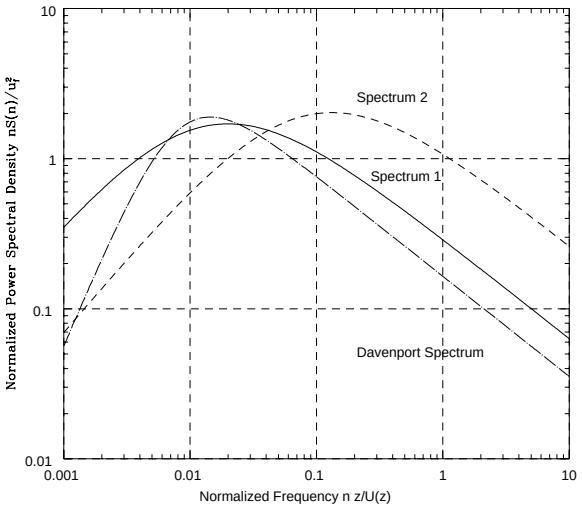

Fig. 8. Theoretical PSD for the velocity wind fluctuations .

The sampling rate of 40 Hz only allows us to study the PSD for frequencies larger than $0.1*(nz/U(z))$; for lower frequencies we will have to sample the wind for a longer time, and in that case the intensity and wind direction may no longer be constant.

For the cases of Mauna Kea and Pico Veleta presented by Antebi et al. (1997), for low frequencies, the wind data show that the normalized power spectrum follows the the general trend of Spectrum 2. The difference of these results may come from differences in the local terrain.

Since the sampling frequency is 40 Hz, the cal-

TABLE 2

PSD PARAMETERS FOR THE SAN PEDRO MÁRTIR WIND DATA

	γ	f_{max}	$<\theta>$	σ_θ	$<m>$
CASE 1	0.956	0.0087	63.5	11.2	0.188
CASE 2	0.690	0.0135	185.6	4.2	0.457
CASE 3	0.625	0.0167	205.9	9.9	0.460
CASE 4	0.627	0.0165	170.3	8.9	0.465
CASE 5	0.969	0.0087	102.6	32.4	0.113

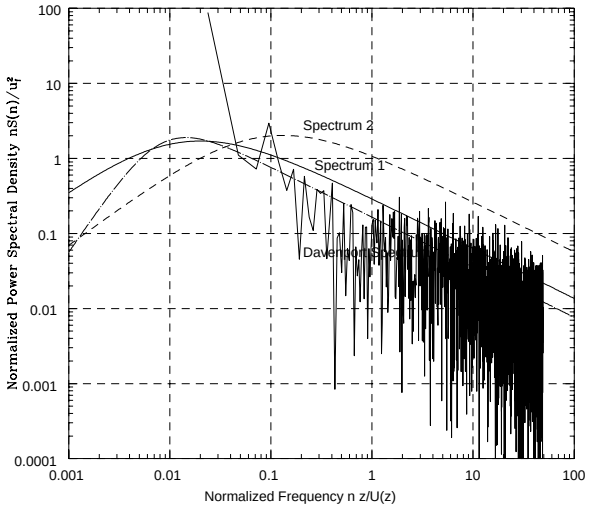

Fig. 10. Same as Figure 9 for **CASE 2**.

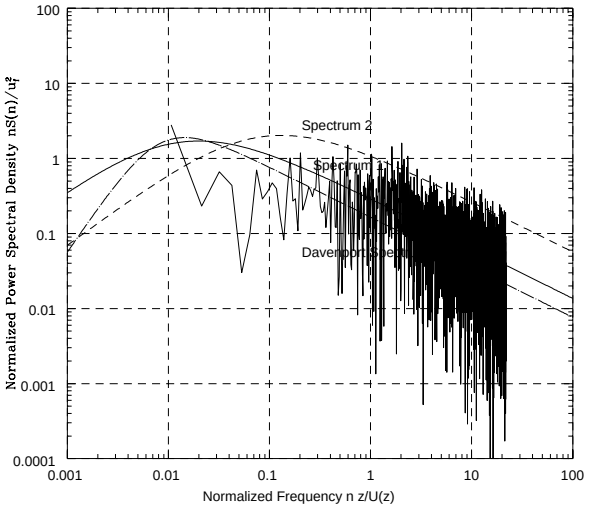

Fig. 12. Same as Figure 9 for **CASE 4**.

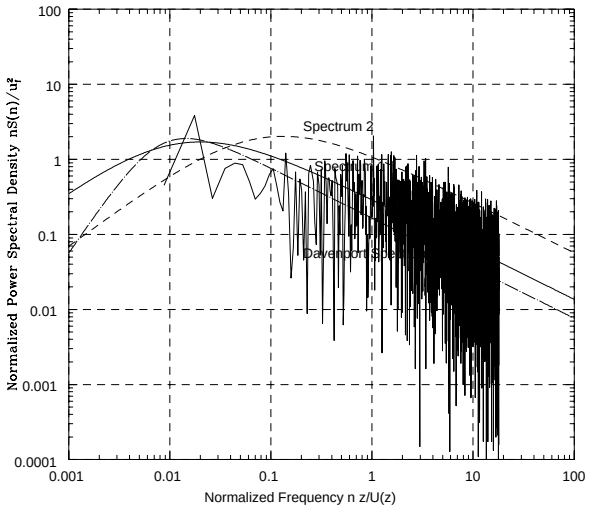

Fig. 11. Same as Figure 9 for **CASE 3**.

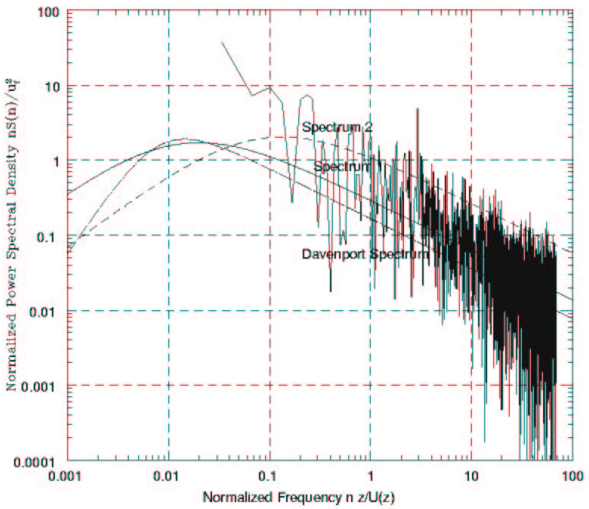

Fig. 13. Same as Figure 9 for **CASE 5**.

culated PSD values for frequencies higher than $f = 200/U(10m)$ Hz may not be considered reliable.

Because the PSD of wind speed fluctuations near ground level is a function of the local terrain roughness, it will be dependent on wind direction. Figure 14 shows the transversal section of the hill in the direction of wind. It shows the altitude of terrain as a function of the displacement in the direction of the wind, $< \theta >$, for the different cases of the wind data. For each case, we define the average steepness of the hill, $< m >$, as the average slope of the hill in that direction. The values of $< m >$ for each case are shown in Table 2.

A power law $\propto f^{-\gamma}$ was fitted to the high fre-

quency part of the PSD in each case, and it was found that the power spectral index γ depends on the direction of the wind through the average slope of the terrain in that direction, $< m >$. With this value for the power law index γ we fitted a Davenport spectrum of the form

$$\frac{n\,S(n)}{u_f^2} \;=\; 4\,\frac{x^2}{(1\,+\,x^2)^{2\gamma}}\;, \qquad (6)$$

to obtain the frequency f_{max} for which the PSD has a maximum in each case. Again, x is defined as before [cf. eq.(3)].

The calculated power index γ and normalized frequency f_{max} for the maximum of the PSD are shown in Table 2. It is noticed that Case 1 and Case 5 with $< m > \sim 0.1$ have a power law index $\gamma \sim 0.9$. Meanwhile, Cases 2 to 4 with high $< m > \sim 0.4$ have $\gamma \sim 0.6$. The steeper the hill the lower is the power law index. It is also found that the steeper the hill the higher the frequency f_{max} at which the PSD has its maximum, Cases 1 and 5 being the ones with the lowest frequencies.

5. CONCLUSIONS

(1) Based on our initial analysis of the selected wind, the power spectral density of the longitudinal wind velocity fluctuations at the site follows a power law ($\propto f^{-\frac{2}{3}}$) for the high frequencies. The behavior at the low frequencies of the spectrum is not clear from the data.

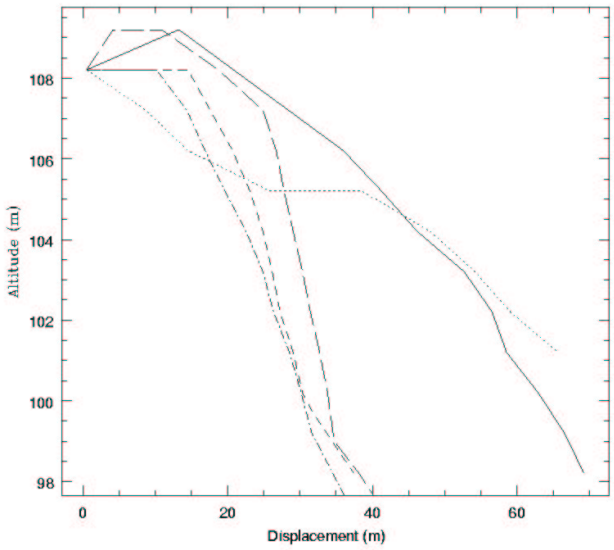

Fig. 14. Transversal sections of the hill (vertical axis) in the direction of the wind $< \theta >$ as a function of the displacement from the anemometer position (horizontal axis) for Case 1 (solid line), Case 2 (short dash), Case 3 (long dash), Case 4 (dot–dash), and Case 5 (dot).

(2) The frequency of the maximum PSD is in the range of 0.008 to 0.017 Hz, so the maximum transfer of energy ocurrs to a very low frequency, of the order of 0.012 Hz. In this way, large structures to be built at this site should have natural frequencies different from these values.

(3) Resonant frequencies were not found in the collected spectrum; all the spectra show a monotonically decreasing behavior after the frequency of maximum power.

(4) The wind spectrum is direction dependent. When the wind blows from a smooth slope of the hill the power index is greater than when the wind blows through a cliff.

(5) From the wind measurements we found that the vertical component of the wind is negligible compared to its longitudinal component. Thus, the energy transfer in the vertical direction may be ignored.

Once the terrain has been leveled to construct the telescope building, the power spectrum of the wind might change and a new study to corroborate these findings may be in order.

We thank W. Schuster for proofreading the typescript and for giving us valuable advice. We acknowledge financial support from the TIM project to acquire the ultrasonic anemometer.

REFERENCES

Antoniou, I., & Asimakopoulos, D. 1992, in Turbulence Measurements on Top of a Steep Hill, Journal of Wind Engineering and Industrial Aerodynamics, 39, 343

Antebi, J., Zarghamee, M. S., & Kan, F. W. 1997, Wind Characterization and Beam Pointing Error - Large Millimeter Telescope, SGH Report to LMT Project Office

Davenport, A. G. 1961, Quart. J. Royal Meteorol. Soc., 87, 194

Kaimal, J. C., Wyngaard, J. C., Izumi, Y., & Coté, O. R, 1972, Quart. J. Royal Meteorol. Soc., 98, 563

Simiu, E., & Scanlan, R. H. 1996, in Wind Effects on Structures: Fundamentals and Applications to Design, 3rd Ed. (New York: Wiley)

Smith, D., Paglioni, T. A., Lovell, A. J., Ukita, N., & Matsuo, H. 2000, Measurements of Dynamic Pointing

Variations of a Large Radio Telescope, Proc. SPIE,
Vol. 4015, p. 467

Benjamín García, David Hiriart, and José Luis Ochoa: Instituto de Astronomía, UNAM, Apartado Postal 877, 22830 Ensenada, B. C., México (hiriart@astrosen.unam.mx).